

# Nanoscale Jet Collision and Mixing Dynamics

Sohail Murad<sup>†</sup> and Ishwar K. Puri<sup>\*,‡</sup>

*Department of Chemical Engineering, University of Illinois at Chicago, Chicago, Illinois 60607, and Department of Engineering Science and Mechanics, Virginia Polytechnic Institute and State University, Blacksburg, Virginia 24061*

*Received December 8, 2006; Revised Manuscript Received January 25, 2007*

## ABSTRACT

Micro- and macroscale investigations have shown that colliding drops always coalesce for small values of the Weber number  $We = \rho U^2 d / \sigma$ . Our molecular dynamic simulations show that nanojets always recoil following head-on collision even though  $We \rightarrow 0$ . The duration between collision and recoil is a function of the nanojet impact velocity  $U_0$  and the nature of intermolecular interactions. Evaporation, which promotes mixing, occurs during recoil and is enhanced by reducing intermolecular interactions. Thereafter, mixing occurs through diffusion. The mixing dynamics are independent of  $U_0$  and the orifice shape. Consistent with a continuum analysis, the characteristic nanojet diameter at stagnation  $d_{s,1} \propto U_0$ , recoil time following collision  $\tau \propto U_0^{-2}$ , and the number of evaporating molecules  $N \propto U_0$ .

Advection-driven fluid interaction and mixing at the nanoscale, while important,<sup>1</sup> remains a relatively unexplored subject. The Reynolds number,  $Re_L = UL/\nu$ , for nanoscale fluid flows is very small due to the miniscule length scales involved (where  $U$  denotes fluid velocity,  $L$  the flow length scale, and  $\nu = \mu/\rho$  the kinematic viscosity). These flows are thus dominated by viscous forces. For water, the viscosity  $\mu \approx 10^{-3}$  Pa s and density  $\rho = 1000$  kg m<sup>-3</sup> so that the viscous force  $\mu^2/\rho \approx 10^{-9}$  N.<sup>2</sup> Because the inertial and time-dependent terms in the Navier–Stokes equations are negligible for inertial matter pushed by a flow at  $Re_L < 1$ , the corresponding viscous force should bring any inertia-induced movement at the nanoscale to rest over a very small distance. The implication is that viscous effects should preclude two fluids from mixing rapidly over a very small lengthscale, i.e., mixing will eventually be diffusion dominated. Herein, we test this hypothesis.

When two flows mix, the advection and diffusive mixing times are, respectively,  $\tau_a \approx O(L/U)$  and  $\tau_d \approx O(L^2/D)$ , where  $D$  represents the binary diffusivity in the medium. When advection dominates,  $\tau_d > \tau_a$ , implying that the flow moves through a distance  $L > D/U$  during the time  $\tau_d$ .<sup>2</sup> Thus, if  $U = 40$  m/s,  $\tau_d = 1.5 \times 10^{-12}$  s (using the value  $D = 2.4 \times 10^{-9}$  m<sup>2</sup> s<sup>-1</sup> for water) so that  $L > 6 \times 10^{-11}$  m (or 0.06 Å). Simulations of a nanoscale mixing process involving high kinetic energy nanojets must therefore be capable of resolving length and time scales that are as small as  $10^{-11}$  m and  $10^{-12}$

s. This is accomplished herein using molecular dynamics (MD) simulations of nanojet collisions. Such simulations are widely used in nanofluidics<sup>3–5</sup> because the usual continuum scale simulations do not accurately predict the flow characteristics at the nanoscale.<sup>3</sup>

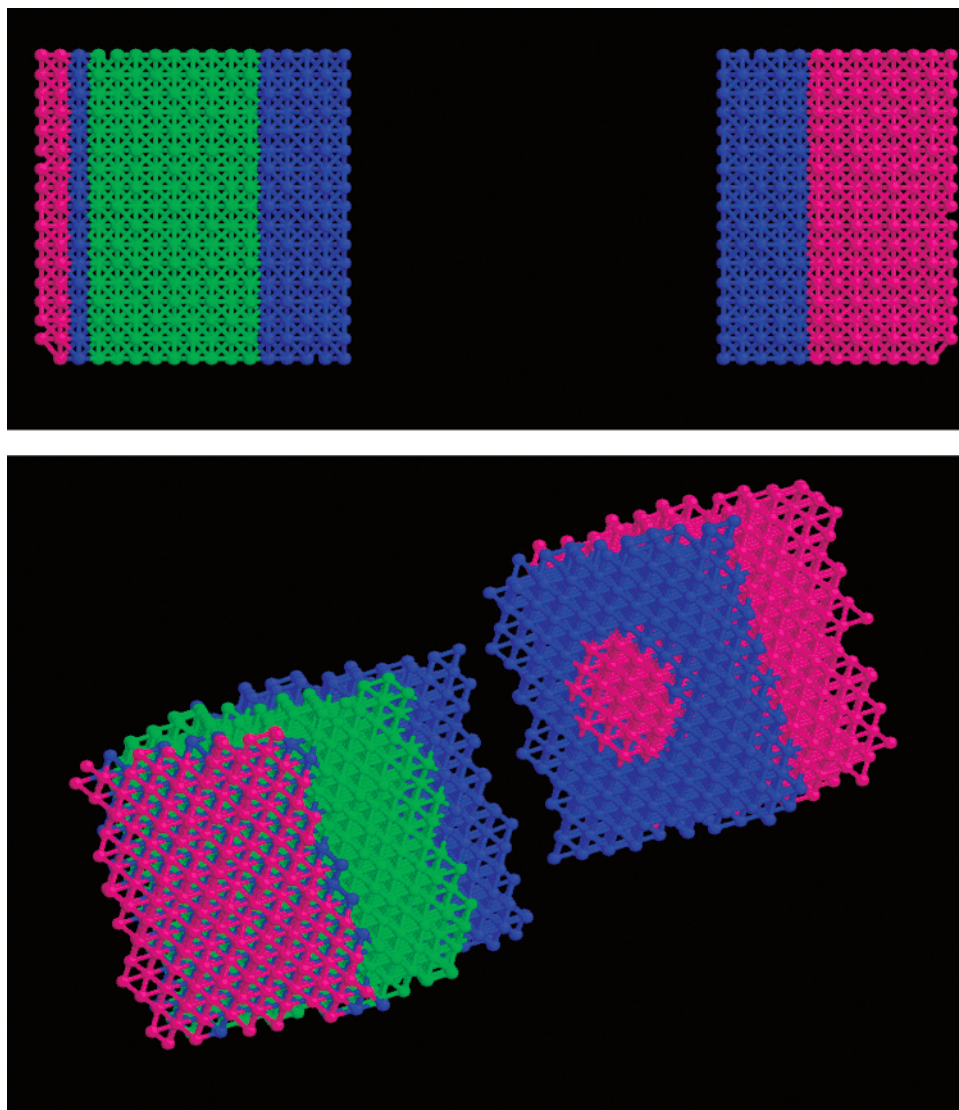
Previous investigations of colliding drops at the micro- and macroscale have shown that drops always coalesce upon collision at small values of the Weber number  $We = \rho U^2 d / \sigma$ <sup>6–9</sup> (where  $\sigma$  denotes the surface tension). Consequently, one method of inducing mixing at the nanoscale could be to induce the head-on collision of ellipsoidal-cap nanojet-type droplets. Consequently, we consider the high-velocity collision dynamics for two similar water nanojets in order to investigate their interaction and subsequent mixing. Such simulations are routine in nanofluidic investigations<sup>10–12</sup> because the usual continuum scale simulations are incapable of predicting the subcontinuum flow characteristics. Nonetheless, as we will show, continuum analogies are useful in understanding the physics of the phenomenon.

The MD simulation methodology has been previously described in detail elsewhere.<sup>13,14</sup> Therefore, it is only summarized here. A Gaussian thermostat maintains constant temperature,<sup>15</sup> and the molecules initially have a Gaussian velocity distribution corresponding to the system temperature. A fifth-order Gear predictor–corrector algorithm for translational motion and a fourth-order predictor–corrector algorithm for rotational motion is used by employing the quaternion method.<sup>15,16</sup> We consider 2494 molecules of water that are initially contained in two reservoirs. The walls of the reservoir are restricted by movable walls that contain five carbon layers, each containing 109 atoms arrayed in an

\* Corresponding author. E-mail: ikpuri@vt.edu.

<sup>†</sup> Department of Chemical Engineering, University of Illinois at Chicago.

<sup>‡</sup> Department of Engineering Science and Mechanics, Virginia Polytechnic Institute and State University.




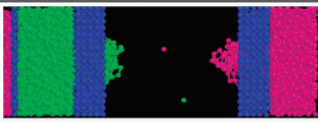
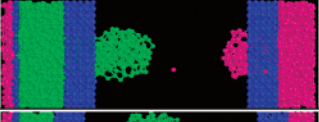
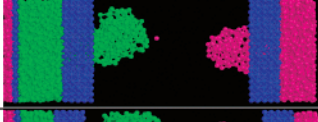



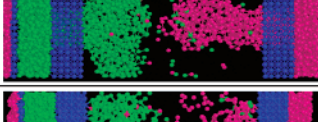

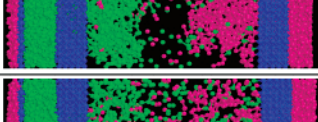

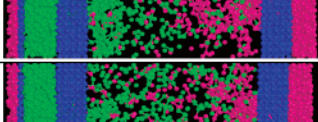
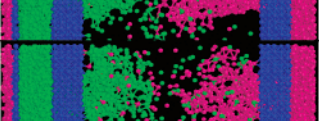
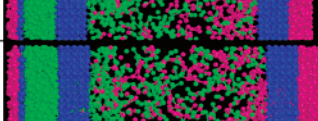
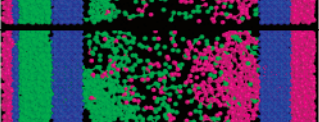
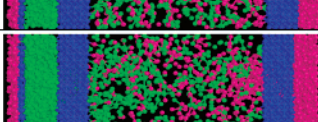
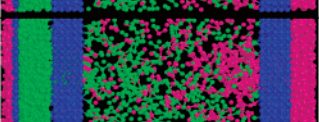
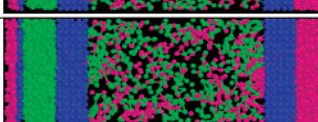
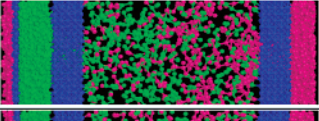
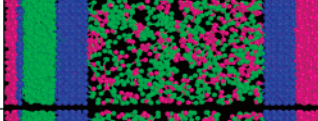
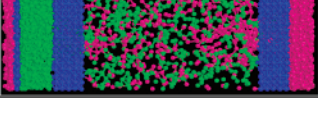
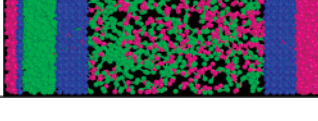
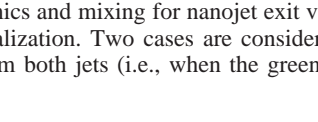
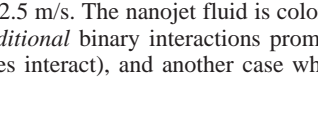
**Figure 1.** Schematic illustration of the simulation system.

fcc lattice. The two reservoirs enclose a cavity that is fully evacuated. The nanojets issue into the cavity through corresponding orifices when the reservoir walls are squeezed. The walls act as the plunger of a syringe would, ejecting fluid through the orifices. The simulations mimic a hypothetical nanoscale laboratory experiment. They are able to readily generate nanojets as small as 1 nm in diameter, which is a dimension that was previously thought to be impossible to reach<sup>12</sup> for molecular fluids such as propane or water (rather than atomic species such as argon).

Figure 1 presents a side ( $y$ - $z$ ) view of the simulations. The blue spheres represent molecules composing the wall membranes, while the green and red symbols represent water molecules emerging from nanojets established, respectively, on the left and right sides. Molecules within an emerging water cluster (as shown in Figure 2) interact due to both Coulombic and van der Waals forces, while water molecules interact with the walls through only van der Waals forces. The domain consists of a parallelepiped with two movable membranes placed at  $x = L_x/4$  and  $3L_x/4$ , where  $L_x$  represents the system size in the  $x$ -direction. It is 9 nm long

( $x$ -direction), and 3 nm wide ( $y$ - and  $z$ -directions). Keeping in mind the periodic boundary conditions, a third membrane, which is always stationary, separates the two fluid reservoirs in the left and right sections of the simulation setup. Including the two water reservoirs at each periphery, the end-to-end dimensions of the simulation box are 11.8 nm  $\times$  3.9 nm (see Figure 1). Each simulation typically runs for  $\approx 2 \times 10^6$  time steps, with each step being  $1.7591 \times 10^{-16}$  s.

Water initially fills both of the peripheral reservoirs. The middle section is initially empty, i.e., it is evacuated. The movable membranes are provided with a specific thickness and geometry. The simulations presented in Figure 2 are for nanojets emerging through an almost circular 1 nm diameter orifice placed in the center of each movable membrane. The molecules constituting the movable membranes are tethered using a simple harmonic potential representing the desired thermal fluctuations of the wall molecules. As these tethering sites are moved, while they continue to undergo thermal fluctuations, a movable membrane is also dragged along toward the system boundaries with constant velocities ( $V_x$ ,

Time, s	Binary interactions	Time, s	No binary interactions
$2.64 \times 10^{-11}$		$2.64 \times 10^{-11}$	
$7.90 \times 10^{-11}$		$7.90 \times 10^{-11}$	
$1.32 \times 10^{-10}$		$1.32 \times 10^{-10}$	
$1.41 \times 10^{-10}$		$1.41 \times 10^{-10}$	
$1.50 \times 10^{-10}$		$1.50 \times 10^{-10}$	
$1.59 \times 10^{-10}$		$1.59 \times 10^{-10}$	
$1.66 \times 10^{-10}$		$1.66 \times 10^{-10}$	
$1.75 \times 10^{-10}$		$1.93 \times 10^{-10}$	
$2.02 \times 10^{-10}$		$2.20 \times 10^{-10}$	
$2.55 \times 10^{-10}$		$2.73 \times 10^{-10}$	
$2.82 \times 10^{-10}$		$2.98 \times 10^{-10}$	
$3.87 \times 10^{-10}$		$4.04 \times 10^{-10}$	

**Figure 2.** Nanojet collision dynamics and mixing for nanojet exit velocities  $U_x = \pm 32.5$  m/s. The nanojet fluid is colored differently (left, green; right, red) for ease of visualization. Two cases are considered, one when *additional* binary interactions promoting mixing occur between the molecules issuing from both jets (i.e., when the green and red molecules interact), and another case when these *additional* interactions are not included.

$-V_x$ ). The resulting compression forces two opposing water nanojets to emerge through the orifices in the centers of these two membranes.

In the simulations, the two movable membranes are displaced at speeds of up to 6 m/s and produce nanojet ejection velocities ( $U_x$ ,  $-U_x$ ) of up to  $\approx 40$  m/s. Water is modeled using the SPC potential,<sup>17</sup> while the membrane atoms are modeled as LJ sites to replicate hydrophobic walls. The water temperature is 298 K. Varying the wall temper-

ature between 298 and 373 K has only a marginal effect on the nanojet ejection rate; hence, only simulations with a 298 K wall temperature are reported. Nanojet formation depends upon the initial velocity of the fluid being ejected from the orifice and the size and shape of that pore. For instance, a too large membrane displacement rate (or fluid compression rate) produces significant lateral fluid transport, resulting in nanojets with an ill-defined axial geometry. On the other hand, too low a displacement rate results in a large almost



spherical water cluster formed near the orifice and adjacent wall surface.

Simulations for two cases, one including an additional binary interaction between water molecules originating from the two nanojets (that further promote mixing) and the other excluding these interactions, are presented in Figure 2. The interactions were implemented by adding a binary interaction parameter  $\zeta_{ij}$  to the usual Lorentz–Berthelot mixing rule<sup>15</sup>  $\epsilon_{ij} = \zeta_{ij}\sqrt{\epsilon_i\epsilon_j}$ . In studies identified as those with additional binary interactions,  $\zeta_{ij}$  was fixed at a value of 2.0 as opposed to the usual value of 1.0 used for the other simulations (without additional binary interactions).

In both cases, head-on collision occurs by  $1.32 \times 10^{-10}$  s. Following collision, additional squeezing of the reservoir through membrane movement is ceased and the nanojet recoils, moving backward toward the orifice. Its motion eventually stagnates after reversing through a recoil length  $L_r$  when it assumes a zero overall velocity. The nanojet recoil is more rapid when there is no additional binary interaction between the molecules contained in the two streams. In the presence of binary interactions, intermolecular interactions promote the formation of molecular clusters due to the presence of additional attractive Van der Waals forces between water molecules emerging from the two jets. Consequently, the colliding jets separate more gradually than when there are no binary interactions.

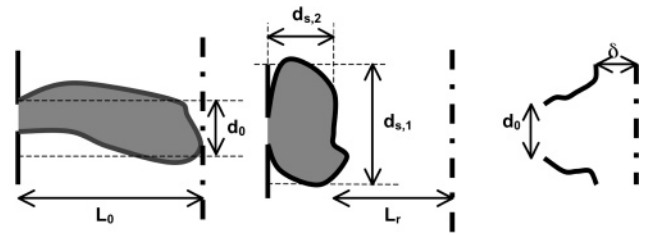
When the two nanojets collide, there is a rapid pressure increase along the collision interface. Here, the impact energy is converted into surface energy and dissipated through viscous effects. The nanojet recoils when its surface energy becomes too large to be sustained. In the presence of attractive intermolecular forces between the two streams (i.e., binary interactions), the conversion of the impact energy into the surface energy occurs over a longer duration. After stagnation, mixing occurs more slowly and is driven by molecular diffusion.

In contrast with previous studies,<sup>6–9</sup> our simulations show that, although the Weber numbers for the nanojets have very small values, they always recoil (or reflexively separate)<sup>6</sup> following head-on collision. If the nanojets are considered to be ellipsoidal cap droplets, then the implication is that the interaction dynamics of colliding drops are different at the nanoscale than at the micro- and macroscales.

The total energy  $E_o$  of a nanojet at the moment of collision consists of the sum of its kinetic and surface energies, respectively  $\rho V U_o^2/2$  and  $\sigma A_o$ , where  $V$  denotes the nanojet volume and  $A_o$  its surface area. After recoiling fully, the nanojet energy  $E_s$  at the first instance of stagnation consists of its surface energy ( $\sigma A_s$ ) alone. An amount  $\Phi$  is dissipated during the recoiling process. Because  $E_o = E_s + \Phi$ ,

$$\Phi = \rho V U_o^2/2 - \sigma(A_s - A_o) \quad (1)$$

Some simplifying assumptions can be made as shown in Figure 3. For instance, although it has an ellipsoidal cap, at the moment of collision, a nanojet can be approximated as having a cylindrical shape that has a diameter  $d_o$  and length  $L_o$ . A nanojet assumes the ellipsoidal shape of a prolate



**Figure 3.** Schematic diagram of the: (a) and (b) Nanojet topology at the moment of impact and after recoil at the instant of stagnation, respectively. The jet characteristic dimension at impact is represented by  $d_o$ , the domain half-length by  $L_o$ , the recoil length by  $L_r$ , and  $d_{s,2} = L_o - L_r$ . (c) Viscous growth layer following nanojet collision.

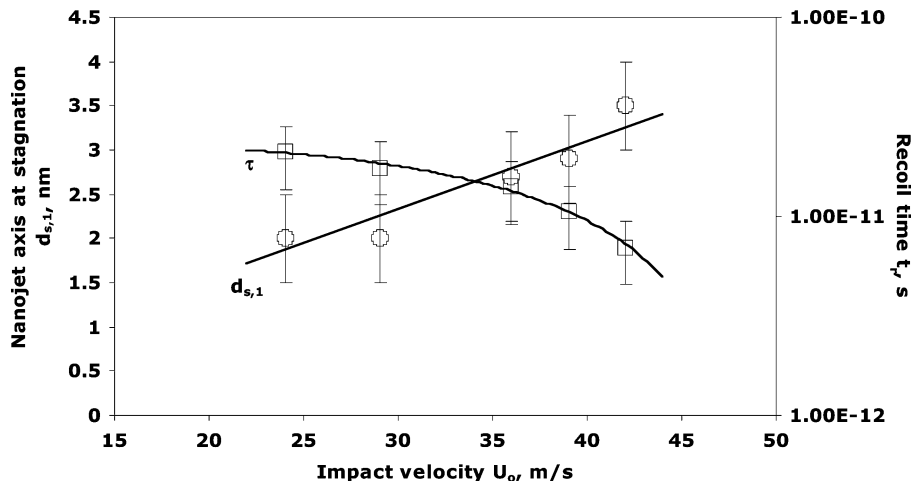
spheroid following collision and recoil (through the distance  $L_r$ ) when it stagnates. At the instant of stagnation, it has an axis of dimension  $d_{s,1}$  transverse to the original flow direction with the other two axes being of length  $d_{s,2}$ .

The behavior of  $\Phi$  can be explained by considering the dissipation relation,<sup>8,18</sup>

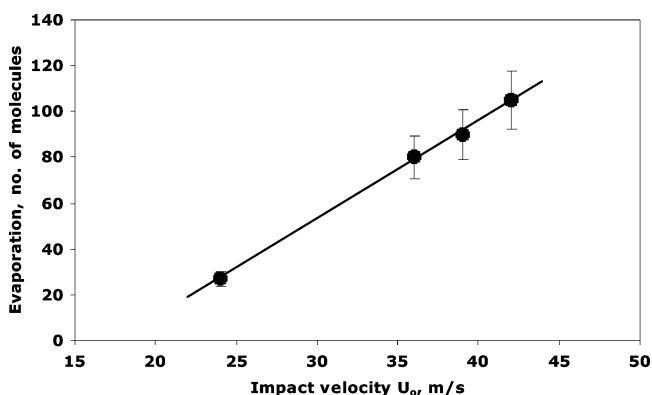
$$\Phi_{1,2} = \mu \int dt \int (1/2)(\partial v/\partial x_j + \partial v/\partial x_i)^2 (dx)^3 \quad (2)$$

At the instant of impact, the jets form a stagnation plane along which fluid rushes away and recoils. The thickness of this layer  $\delta$  depends upon viscous growth and forms the basis for the largest velocity gradient  $U_o/\delta$ . Equating the viscous stress to the dynamic pressure,  $\mu U_o/\delta \approx \rho U_o^2/2$ ,  $\delta \approx 2\mu/(\rho U_o)$ .<sup>18</sup> The thinner the viscous layer, the more fluid is squeezed axially. Hence, if the participating volume at the interface of a colliding nanojet is constant, then  $d_{s,1} \propto (1/\delta)$ , i.e.,  $d_{s,1} \propto U_o$ . Viscous dissipation initially occurs in a small disk-like volume  $\pi d_o^2 \delta/4$  that is adjacent to the boundaries of the colliding nanojets. Because  $\delta \approx (\nu\tau)^{1/2}$ , the characteristic deformation (or recoil) time  $\tau \approx 4\mu/(\rho U_o^2)$ . For the nanojets to separate, this recoil time should be faster than the characteristic coalescence time  $\tau_c \approx \mu d_o/\sigma \approx (We/Re)(d_o/U_o)$ .<sup>19,20</sup>

In Figure 4, we present the variation of  $d_{s,1}$  and the recoil time  $\tau$  with respect to the nanojet velocity  $U_o$  at the moment of impact. As expected, the ellipsoid axis has a linear dependence on  $U_o$  through the relation  $d_{s,1} = 7.72 \times 10^{-11} U_o$  m. In addition, the nanojet recoil time roughly follows the relation  $\tau = 6 \times 10^{-9}/U_o^2$ . Both results are in accord with the analytical relations that are based on a continuum approach. The utility of comparing a continuum approach with the results of nanoscale MD fluid simulations has been previously stated. For instance, the hydrodynamic forces simulated on a carbon nanotube have been found to be in good agreement with the macroscopic Stokes–Oseen solution for the flow past an array of circular cylinders.<sup>21–25</sup> The implication of such studies is that nanoscale fluid flow problems do not always occur below the smallest continuum scale. Because a point function, such as density, based on a continuum approach, is an average property, it could be adequately described provided the nanoscale volume of interest contains a sufficient number of molecules.



**Figure 4.** Variation of the nanojet characteristic dimension at stagnation and recoil time with nanojet velocity. Binary interactions were not considered for these simulations.



**Figure 5.** Number of molecules evaporated for various impact velocities. Binary interactions were not considered for these simulations.

Substituting the expressions for the maximum velocity gradient, deformation time and dissipation volume in eq 2,

$$\Phi_1 \approx (\pi d_o^2/4)(\mu U_o) \quad (3)$$

The local interfacial pressure increases when the nanojets collide, compressing the volume along the interface. As the energy dissipates and the pressure relaxes, the local volume increases, which is seen in the simulations through the evaporation of the water molecules. Here, we consider individual molecules that break away from a cluster as having evaporated. We thereafter infer the amount of evaporation from the simulations by monitoring the separation of individual molecules from the contiguous fluid mass. Larger impact velocities lead to increasing dissipation (and therefore greater evaporation), as shown in Figure 5.

The figure shows that, in accord with eq 3 (again, a continuum relation), the total number of evaporated water molecules  $N$  (determined at the instant the nanojets stagnate after recoiling) scales linearly with the impact velocity according to the relation  $N = 4.3U_o - 76$ . The evaporation can also be explained on a thermodynamics basis by considering a constant mass system that exists at a specified

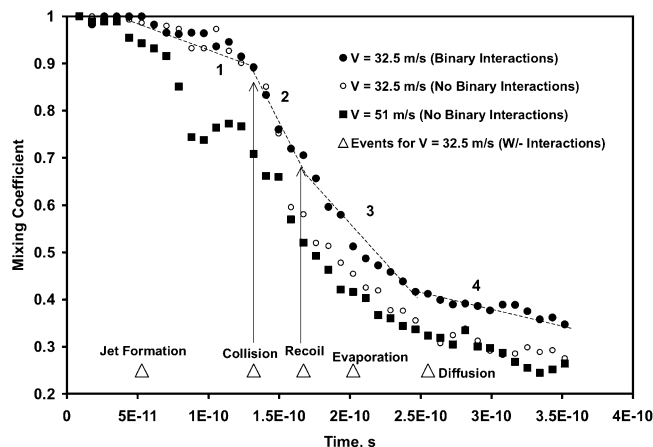
temperature and pressure. When the system is perturbed with respect to pressure, stability considerations imply that  $((\partial^2 G / \partial P^2)_T = (\partial V / \partial P)_T) < 0$ , where  $G$  denotes the Gibbs energy and  $T$  and  $P$  represent temperature and pressure.<sup>17</sup> Consequently perturbations that increase the pressure decrease the volume and vice versa. The relaxation of local pressure during energy dissipation favors evaporation.

A mixing parameter,

$$M(t) = \sum_{i=1}^N [(x_i(t) - c(t))^2] \quad (4)$$

has been used to quantify the extent of nanoscale mixing. Here,  $x_i(t)$  denotes the composition of component  $\alpha$  contained in thin strips (1, 2, ...,  $N$ ) that are stacked in the direction in which mixing is being measured. The water molecules in the two nanojets are considered as separate components for the purpose of this mixing analysis. In our setup, the  $x$  coordinate (the direction in which the nanojets move) is an obvious choice; we measure mixing from left to right. In eq 4,  $c(t)$  denotes the average composition of  $\alpha$  between the two orifices. For complete mixing, the composition of  $\alpha$  in each slit would equal  $c(t)$  so that  $M(t) = 0$ . In the absence of mixing,  $M(t)$  would have a constant value depending on the number of strips  $N$ . If convenient, the parameter could be further normalized by  $N$  or  $M(0)$ .

Figure 6 presents the time evolution of  $M$  ( $= M(t)/M(0)$ ) for two initial jet exit velocities, i.e., 32.5 and 51 m/s. The first two results in the figure correspond to the visualizations presented for both cases in Figure 2. A larger jet exit velocity reduces the nanojet collision time but does not improve the overall mixing rate following impact, either through evaporation or diffusion (cf. Figure 4). Evaporation is less favored when mixing is energetically neutral (i.e., additional binary interactions exist between the water molecules originating in the two nanojet streams). In all cases (i.e., in presence and absence of interactions, and higher and lower velocities), the overall qualitative features of the mixing dynamics are similar.



**Figure 6.** Impact of nanojet exit velocity  $U_x$  on mixing in terms of a mixing parameter.

The evolution of  $M$  occurs through four transitions, as shown in Figure 6 through various events for the 32.5 m/s case that includes binary interactions (case 1). There is little change in the  $M$  value during the nanojet formation stage prior to collision (denoted as period 1 in the figure). The nanojets recoil following collision. The time between collision and recoil during period 2 is a function of the impact velocity and the nature of intermolecular interactions between the two streams. Evaporation occurs in period 3 during recoil until the nanojets stagnate, which promotes mixing. Thereafter, mixing occurs through diffusion, which is a much slower process during period 4. Eliminating the binary intermolecular interactions between the two streams reduces the duration of period 2. In this case, evaporation occurs sooner and is also enhanced. The net result is a  $\approx 20\%$  decrease in the value of  $M$  from the corresponding value for case 1. A simulation for an identical system with a square orifice of 1 nm side provided similar results as for case 1. While jet formation in the two cases is somewhat different, the mixing dynamics are similar. The results show that, while viscous effects are dominant at the nanoscale so that mixing is eventually facilitated by diffusion, it also occurs through evaporation during nanojet recoil due to dissipation effects.

In conclusion, our results show that fluid mixing occurs when liquid nanojets recoil following collision. The time taken for liquid nanojets to recoil after collision decreases when binary intermolecular attractions between the two streams are reduced. Liquid evaporation occurs during the recoil period until the nanojets stagnate. Thereafter, mixing

occurs solely through molecular diffusion, which is much slower. Consequently, while nanoscale mixing is eventually diffusion-limited, it can also occur through evaporation during nanojet recoil, which is induced through energy dissipation. A larger jet exit velocity reduces the nanojet collision time but does not improve the overall mixing rate following impact. Likewise, the mixing dynamics appear to be independent of the orifice shape. Contrary to previous micro- and macroscale investigations, our simulations show that nanojets always recoil (or reflexively separate) following head-on collision, even though  $We \rightarrow 0$ . Hence, the interaction dynamics of colliding drops appear to be different at the nanoscale. We find that continuum analogies are useful to understand nanoscale phenomenon. For instance, we find that, consistent with a continuum analysis, the characteristic stagnant nanojet diameter  $d_{s,1} \propto U_o$ , recoil time  $\tau \propto U_o^{-2}$ , and the number of evaporating molecules  $N \propto U_o$ .

## References

- (1) Knight, J. B.; Vishwanath, A.; Brody, J. P.; Austin, R. H. *Phys. Rev. Lett.* **1998**, *80*, 3863.
- (2) Purcell, E. M. *Am. J. Phys.* **1977**, *45*, 3.
- (3) Qiao, R.; Aluru, N. R. *Colloids Surf., A* **2005**, *267*, 103.
- (4) Düren, T.; Keil, F. J.; Seaton, N. A. *Chem. Eng. Sci.* **2002**, *57*, 1343.
- (5) Hanasaki, I.; Nakatani, A.; Kitagawa, H. *Sci. Technol. Adv. Mater.* **2004**, *5*, 107.
- (6) Ashgriz, N.; Poo, J. Y. *J. Fluid Mech.* **1990**, *221*, 183.
- (7) Jiang, J.; Umemura, A.; Law, C. K. *J. Fluid Mech.* **1992**, *221*, 183.
- (8) Qian, J.; Law, C. K. *J. Fluid Mech.* **1997**, *331*, 59.
- (9) Willis, K.; Orme, M. *Exp. Fluids* **2003**, *34*, 28–41.
- (10) Koplik, J.; Banavar, R. *Phys. Fluids A* **1992**, *5*, 521.
- (11) Kawano, S. *Phys. Rev. E* **1998**, *58*, 4468.
- (12) Mozeler, M.; Landman, U. *Science* **2000**, *289*, 1165.
- (13) Murad, S.; Lin, J. *Chem. Eng. J.* **1999**, *74*, 99.
- (14) Murad, S.; Lin, J. *Ind. Eng. Chem. Res.* **2002**, *41*, 1076.
- (15) Allen, M. P.; Tildesley, D. J. *Computer Simulation of Liquids*; Clarendon Press: Oxford, 1987.
- (16) Evans, D. J.; Murad, S. *Mol. Phys.* **1977**, *34*, 327.
- (17) Berendsen, H. J. C.; Postma, J.; Gunsteren, W. F. In *Intermolecular Forces*; Pullman, B., Ed.; Reidel: Dordrecht, The Netherlands, 1981.
- (18) Chiu, S.-L.; Li, T.-H. *Phys. Fluids* **2005**, *17*, 122103.
- (19) Frenkel, J. *J. Phys.* **1945**, *9*, 385.
- (20) Zachariah, M. R.; Carrier, M. J. *J. Aerosol Sci.* **1999**, *30*, 1139.
- (21) Walther, J. H.; Werder, T.; Jaffe, R. L.; Koumoutsakos, P. *Phys. Rev. E* **2004**, *69*, 062201.
- (22) Marmanis, H.; Thoroddsen, S. T. *Phys. Fluids* **1996**, *8*, 1344.
- (23) Clift, R.; Grace, J. R.; Weber, M. E. *Bubbles, Drops, and Particles*; Academic Press: New York, 1978; pp 187–188.
- (24) Fukai, J.; Miyatake, O.; Shiiba, Y.; Yamamoto, T.; Poulikakos, D.; Megaridis, C. M.; Zhao, Z. *Phys. Fluids A* **1993**, *5*, 2588.
- (25) Annamalai, K.; Puri, I. K. *Advanced Thermodynamics Engineering*; CRC Press: Boca Raton, FL, 2002; p 491.

NL062887O